

A Distributed Scalable Architecture using \mathcal{L}_1 Adaptive Controllers for Primary Voltage Control of DC Microgrids

Daniel O’Keeffe^{*†1}, Stefano Rivero^{‡2}, Laura Albiol-Tendillo^{§2}, and Gordon Lightbody^{¶1,3}

¹Control & Intelligent Systems Group, School of Engineering, University College of Cork, Ireland

²United Technologies Research Centre Ireland Ltd, 4th Floor Penrose Business Centre, Cork, Ireland

³MaREI-SFI Research Centre, University College Cork, Ireland

Technical Report
January, 2018

Abstract

This paper proposes a new distributed control architecture for distributed generation units in heterogeneous DC islanded microgrids. Each unit is equipped with state-feedback baseline and augmenting \mathcal{L}_1 adaptive voltage controllers at the primary level of the microgrid control hierarchy. Local controller synthesis is scalable as it only requires information about corresponding units, couplings, and at most, the addition of state-predictor measurements of neighbouring controllers. Global asymptotic stability of the microgrid is guaranteed in a plug-and-play fashion by exploiting Lyapunov functions and algebraic Riccati equations. The performance of the proposed architecture is evaluated using a heterogeneous DC islanded microgrid that consists of 6 DC-DC boost converters configured in a radial and meshed topology. The use of \mathcal{L}_1 adaptive controllers achieves fast and robust microgrid voltage stability in the presence of plug-and-play operations, topology changes and unknown load changes. Finally, the distributed architecture is tested on a bus-connected islanded-microgrid consisting of linear resistive load and non-linear DC motor.

Keywords: *Distributed Control, Low-Voltage DC Islanded Microgrid, Robust-Adaptive Control, Scalable Design, Voltage Stability*

*Research is supported by the Irish Research Council enterprise partnership scheme (Award No. R16920) in collaboration with University College Cork, Ireland and United Technologies Research Centre Ireland Ltd.

[†]Email: danielokeeffe@umail.ucc.ie; Corresponding author

[‡]Email: RiversS@utrc.ucc.com

[§]Email: AlbiolL@utrc.ucc.com

[¶]Email: g.lightbody@ucc.ie

1 Introduction

Advances in DC-DC power electronics, has led to the promising emergence of DC islanded microgrids (ImGs) [1]. DC power distribution can avoid inherent issues associated with AC such as harmonic compensation, reactive power and synchronisation; thus improving power quality, efficiency and reliability. Furthermore, the use of DC can reduce the weight of traditional AC power networks by 10 tons/MW [1]; which is important for electric vehicle and aircraft applications. Recently, DC ImGs have been deployed in low-voltage DC (LVDC) networks such as telecommunication towers, occupied interior spaces, data centres and traction systems [2–5]. The next wave of DC ImG applications are expected in large-scale residential, commercial and industrial buildings, and aerospace [6–8].

The proliferation of mGs has led to a growing importance in the development and commercialisation of mG control systems to ensure safe and efficient operation [9]. Over recent years, increasing complexities within large-scale systems (LSS) has led to demands for local and scalable algorithms that can coordinate global performance [10]. Thus, decentralised and distributed control architectures have become an attractive alternative to centralised approaches [11–14]. Currently, mG control system manufacturers/vendors offer monolithic solutions i.e. a fixed system with limited flexibility and robustness to uncertainty, as outlined in [15, 16]. Many control solutions utilise proprietary platforms which require extensive design details on behalf of vendors. Though proprietary designs are standardised and reliable, this approach increases capital and operational expenditure, commissioning time and complexity of the mG design [17]. Additionally, some key features of autonomous mGs include; the economic dispatch of DGUs, the reduction of operating and maintenance costs, and healthy levels of load-servicing and reserve capacity. As a result, there is a growing trend towards mG control solutions that allow plug-and-play (PnP) capabilities to enable system owners the scalability, flexibility and accessibility to implement and maintain controls in LSS.

PnP control designs, first outlined in [18], have successfully been deployed as primary and secondary controllers in the standard hierarchical control structure of AC [19, 20] and DC ImGs [21–23]. Primary controllers are locally responsible for stable power distribution, while secondary controllers coordinate system voltage levels and improve load-sharing accuracy using low-bandwidth communications (LBC). PnP controllers maintain operation stability when DGUs and loads are reconfigured without requiring *a priori* knowledge. Global asymptotic stability (GAS) is guaranteed by checking the viability of DGU plug-in/out operations through a local optimisation problem using linear matrix inequalities (LMIs). Furthermore, the technique is scalable as local controllers depend only on knowledge of corresponding DGU and line-couplings. Once DGU plug-in/out, neighbouring controllers are required to retune off-line, resulting in limited robustness. Recently, line-independent [24] and robust [25] PnP controllers were proposed to overcome this. However, these PnP techniques are computationally extensive, controller gains are required to discontinuously switch after off-line stability checks are performed, and robustness to network uncertainty is limited.

Adaptive control schemes have recently been proposed to extend performance and functionality within heterogeneous and uncertain large-scale mGs. As market deregulation continues and system owners achieve greater flexibility, mGs will become increasingly heterogeneous; consisting of different DGUs/DSUs, topologies, unknown loads, communications and operations. Thus, architectural and network uncertainty will influence the coordination and control of large-scale mGs. Fast and robust performance can be guaranteed in the presence of uncertainty and changing dynamics by incorporating adaptive control techniques that utilise Lyapunov stability theory [26]. In [27–31], adaptation is introduced to the primary and secondary controllers. However, these strategies are based on premeditated conditions or linear controllers to provide small-signal adjustments to droop coefficients for dynamic performance when achieving system objectives such as voltage restoration and load-sharing. Furthermore, these strategies depend on accurate system models, specific mG topologies, and do not address well-documented adaptive control problems, as outlined in [32]. Historically, adaptive control techniques, particularly the model reference adaptive controller (MRAC), faced difficulties with regards to practical implementation. Though

adaptive systems can be found throughout nature, ensuring robustness and fast adaptation in the presence of unknown, time-varying dynamics proved difficult to predict and guarantee. Such limitations led to recent advancements in robust-adaptive control, including closed-loop reference model (CRM) and \mathcal{L}_1 adaptive control (\mathcal{L}_1 AC) techniques [33, 34].

The CRM adaptive controller uses a closed-loop reference model in order to guarantee stability and improve transient responses within uncertain environments. The first work to perform a comprehensive stability analysis of a DC ImG incorporating adaptive controllers is found in [35, 36]. This work also adjusts the droop coefficients using distributed CRM adaptive secondary controllers. Droop control is an inertial controller, and thus adaptation will reactively act on state deviations within the system. Here, the adaptive laws are adapting to uncertainty of the droop coefficients, as opposed to uncertainty concerning the system dynamics. Moreover, rapidly changing dynamics such as PnP operations are not facilitated. Ultimately, [35, 36] require the design of adaptive controllers for each global objective i.e. voltage balancing and load-sharing. By performing robust adaptation at the primary level, the number of adaptive controllers is reduced to one, and a more simplified hierarchical control structure, such as the non-droop control coordination layer in [22, 23], can be designed thereafter.

This paper proposes a new scalable distributed adaptive architecture at the primary control level of DC ImGs. The \mathcal{L}_1 AC is proposed as it has achieved promising success in practical applications [37–41]. Local DC-DC boost power converters are equipped with decentralised state-feedback (DeSSf) baseline controllers and augmented with \mathcal{L}_1 adaptive voltage controllers. The rationale for implementing an augmentation approach as opposed to a fully adaptive one is that in real systems it is common to have baseline controllers designed to provide reference tracking and disturbance rejection during nominal operation [37, 38, 42]. This approach can also facilitate greater flexibility to a system owner as previously discussed. The distributed architecture is shown to achieve robust voltage control which adheres to IEEE transient and steady-state performance standards of [43]. The architecture is evaluated within the context of;

- Heterogeneous DC ImG consisting of DC-DC boost converters.
- Arbitrary topologies; radial, meshed and bus-connected.
- Parametric uncertainty of converter, coupling and unknown load dynamics.
- Reconfiguration of DGUs through PnP operations and online topology changes due to line faults.

This work follows on from our previous work implementing a decentralised \mathcal{L}_1 AC architecture within DC ImGs [44] by guaranteeing GAS in a PnP fashion. Following [44], GAS can be ensured off-line in a centralised fashion using aggregated vector Lyapunov functions. However, this approach leads to conservative designs; controllers require retuning, as shown in [15]. Furthermore, determining the correct controllers to retune can prove difficult as the mG size increases in LSS. The distributed architecture instead guarantees GAS by solving local algebraic Riccati equations (AREs), as outlined in [45–47]. Consequently, the architecture requires the local \mathcal{L}_1 ACs to measure the states of each neighbouring \mathcal{L}_1 AC. Conveniently, this LBC flow has the same topology as the coupling graph, and as a result, the architecture remains scalable.

The paper is organised as follows. In section 2, the DC ImG model is developed and baseline controllers are designed. Section 3 details the design and GAS analysis of the distributed \mathcal{L}_1 AC architecture. Finally, section 4 demonstrates the effectiveness of the proposed designs using radial, meshed and bus-connected DC ImG topologies to conduct PnP, topology change and load disturbance tests.

A version of this work has been submitted to IEEE Transactions on Smart Grid.

2 DC Islanded Microgrid Model

This work considers boost converters, which step-up low-voltages to high-voltages. Boost converter controllers are notoriously difficult to tune in mGs due to their non-minimum phase

action and have only received attention recently [15], [25]. As proposed in [21], the DC ImG is modelled as a two-node network for control orientated design. Subsequently, the network is generalised to N -nodes. The ImG of Fig. 1 is arranged in an arbitrary load-connected topology, where each DGU supplies power to a local load at the point of common coupling (PCC). DGUs can be mapped to load-connections via the Kron Reduction method [48], which preserves the profile of electrical parameters at the PCC regardless of the topology. This is a positive feature, as the model of each DGU is not dependent on the load, which could be unknown e.g. non-linear/linear resistive, interfacing buck converter or constant power load. Instead, Fig. 1 represents the load as a current disturbance, I_{Li} . Each DGU is controlled by adjusting the duty-cycle d_i of a solid-state switch using pulse-width modulation (PWM). Fig. 1 represents the averaged dynamics of two coupled boost converters, i and j , over both on/off switching states. DGUs are coupled via resistive and inductive power lines.

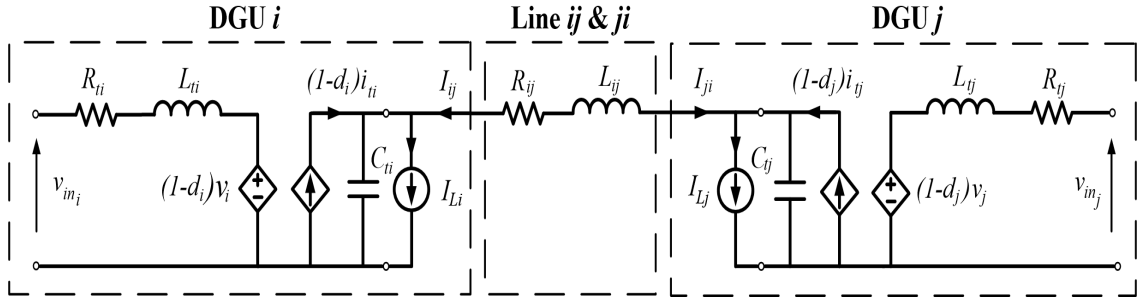


Figure 1: Averaged nonlinear model of DC ImG composed of two coupled boost converter DGUs with unknown loads.

Applying Kirchoff's voltage and current laws to the DC ImG of Fig. 1 yields the following set of averaged differential equations:

$$\text{DGU } i: \begin{cases} \frac{dI_{ti}}{dt} = \frac{1}{L_{ti}} V_{in_i} - \frac{(1-d_i)}{L_{ti}} V_{dc_i} - \frac{R_{ti}}{L_{ti}} I_{ti} \\ \frac{dV_{dc_i}}{dt} = \frac{(1-d_i)}{C_{ti}} I_{ti} + \frac{1}{C_{ti}} I_{ij} - \frac{1}{C_{ti}} I_{Li} \end{cases} \quad (1a)$$

$$\text{DGU } j: \begin{cases} \frac{dI_{tj}}{dt} = \frac{1}{L_{tj}} V_{in_j} - \frac{(1-d_j)}{L_{tj}} V_{dc_j} - \frac{R_{tj}}{L_{tj}} I_{tj}, \\ \frac{dV_{dc_j}}{dt} = \frac{(1-d_j)}{C_{tj}} I_{tj} + \frac{1}{C_{tj}} I_{ji} - \frac{1}{C_{tj}} I_{Lj} \end{cases} \quad (1b)$$

$$\text{Line } ij: \left\{ L_{ij} \frac{dI_{ij}}{dt} = V_{dc_j} - R_{ij} I_{ij} - V_{dc_i} \right. \quad (1c)$$

$$\text{Line } ji: \left\{ L_{ji} \frac{dI_{ji}}{dt} = V_{dc_i} - R_{ji} I_{ji} - V_{dc_j} \right. \quad (1d)$$

Assumption 1: To ensure $I_{ij}(t) = -I_{ji}(t) \forall t \geq 0$, initial line current states are defined as $I_{ij}(0) = -I_{ji}(0)$. With this, $R_{ij} = R_{ji}$ and $L_{ij} = L_{ji}$.

2.1 Quasi Stationary Line Model

If the time constant of the line transients is very fast, i.e. assuming L_{ij} and L_{ji} are significantly small, then line dynamics can be neglected. This type of model is known as a Quasi-Stationary Line (QSL) approximation. This is usually a good approximation for small-scale mGs where the lines are predominantly resistive. In open-loop, global stability can be inferred by ensuring local DGU stability, as detailed in section 6.1 of [44]. Line equations (1c) and (1d) are represented in steady-state form using QSL approximations, i.e. $\frac{dI_{ij}}{dt} = \frac{dI_{ji}}{dt} = 0$:

$$I_{ij} = \frac{V_{dc_j} - V_{dc_i}}{R_{ij}}, \quad (2)$$

$$I_{ji} = \frac{V_{dc_i} - V_{dc_j}}{R_{ji}}. \quad (3)$$

Replacing line current variable I_{ij} of equation (1a) with equation (2) yields the following model for DGU i ,

$$\text{DGU } i: \begin{cases} \frac{dI_{ti}}{dt} = \frac{1}{L_{ti}}V_{in_i} - \frac{(1-d_i)}{L_{ti}}V_{dc_i} - \frac{R_{ti}}{L_{ti}}I_{ti} \\ \frac{dV_{dc_i}}{dt} = \frac{(1-d_i)}{C_{ti}}I_{ti} + \frac{V_{dc_j}}{R_{ij}C_{ti}} - \frac{V_{dc_i}}{R_{ij}C_{ti}} - \frac{1}{C_{ti}}I_{Li} \end{cases} \quad (4)$$

Interchanging indexes i and j yields the model for DGU j . Representing (4) in a general compact state space form, the dynamics of DGU i are,

$$\Sigma_{[i]}^{\text{DGU}}: \begin{cases} \dot{x}_{[i]}(t) = \begin{bmatrix} -\frac{R_{ti}}{L_{ti}} & -\frac{(1-d_i)}{L_{ti}} \\ \frac{(1-d_j)}{C_{ti}} & -\frac{1}{R_{ij}C_{ti}} \end{bmatrix} x_{[i]}(t) + \begin{bmatrix} \frac{1}{L_{ti}} \\ 0 \end{bmatrix} V_{in_i} + \begin{bmatrix} 0 \\ -\frac{1}{C_{ti}} \end{bmatrix} I_{Li} + \begin{bmatrix} 0 & 0 \\ 0 & \frac{1}{R_{ij}C_{ti}} \end{bmatrix} x_{[j]}(t) \\ y_{[i]}(t) = C_i x_{[i]}(t) \end{cases} \quad (5)$$

where $x_{[i]}(t) = [I_{ti}, V_{dc_i}]^T$, I_{Li} is the exogenous current disturbance. Unlike with the buck converter, where the averaged state space model of (5) is equivalent to the small-signal state space model, the boost converter is different. From the state matrix of above, the duty-cycle control input is a product of the state vector. As a result, the duty-cycle operating point directly influences stability. The averaged model is therefore non-linear and must be linearised about the duty-cycle operating point by forming a small-signal model¹.

$$\Sigma_{[i]}^{\text{DGU}}: \begin{cases} \dot{\tilde{x}}_{[i]}(t) = A_{ii}\tilde{x}_{[i]}(t) + B_i u_{[i]}(t) + E_i d_{[i]}(t) + \zeta_{[i]}(t) + \gamma_{[i]}(t) \\ y_{[i]}(t) = C_i \tilde{x}_{[i]}(t) \end{cases} \quad (6)$$

where $x_{[i]}(t) = [\tilde{i}_{ti}, \tilde{v}_{dc_i}]^T$, is the small-signal state vector, $u_{[i]}(t) = \tilde{d}_i(t)$ is the small-signal PWM control signal, $d_i(t) = \tilde{i}_{Li}$ is the small-signal exogenous current disturbance, $\zeta_{[i]}(t) = A_{ij}x_j(t)$ represents coupling with DGU j and $\gamma_i(t) = \frac{\tilde{v}_{in_i}}{L_{ti}}$ is the small-signal input voltage disturbance. It is assumed that changes in input voltages V_{in_k} are very slow, and thus can be neglected². Therefore $\gamma_i(t) = 0$.

¹Note: each average quantity can be expressed as the sum of its steady state and small-signal values e.g. $d_k = D_k + \tilde{d}_k$, $V_{dc_k} = \bar{V}_{dc_k} + \tilde{v}_{dc_k}$.

²As the input voltage to power converters in a mG is usually from renewable power or storage devices. The dynamics of these devices are much slower than the fast switching dynamics of power converters, therefore it is a safe assumption to neglect small-signal changes in input voltage

The matrices of (6) are,

$$A_{ii} = \begin{bmatrix} -\frac{R_{ti}}{L_{ti}} & -\frac{(1-D_i)}{L_{ti}} \\ \frac{(1-D_i)}{C_{ti}} & -\frac{1}{R_{ij}C_{ti}} \end{bmatrix} A_{ij} = \begin{bmatrix} 0 & 0 \\ 0 & \frac{1}{R_{ij}C_{ti}} \end{bmatrix} B_i = \begin{bmatrix} \frac{\bar{V}_{dc_i}}{L_{ti}} \\ -\frac{\bar{I}_{ti}}{C_{ti}} \end{bmatrix} E_i = \begin{bmatrix} 0 \\ -\frac{1}{C_{ti}} \end{bmatrix} C_i = \begin{bmatrix} 0 & 1 \end{bmatrix}$$

$$\text{where } \bar{V}_{dc_i} = \frac{\bar{V}_{in_i}}{(1-D_i)} \text{ and } \bar{I}_{ti} = \frac{\bar{V}_{in_i}}{(1-D_i)^2 R_{L_i}}.$$

2.2 QSL Model DC Islanded Microgrid Composed of N DGUs

In this section, the two DGU network of Fig. 1 is generalised to an ImG composed of N converter DGUs. [15] demonstrated that converter coupling dynamics predominantly manifest from physical power lines; duty-cycle coupling is weak. Neighbouring DGUs are thus defined if they are coupled by the RL power line of Fig. 1. Letting $\mathcal{D} = \{1, \dots, N-1\}$, $\mathcal{N}_i \subset \mathcal{D}$ denotes a neighbour-subset for DGU i . As before, assuming QSL approximation of all line dynamics $(i, j) \in \mathcal{D}$, the DC ImG model is represented by (5), with $\zeta_{[i]}(t) = \sum_{j \in \mathcal{N}_i} A_{ij} x_{[j]}(t)$. The only change in (5) is the local state vector matrix A_{ii} , becoming:

$$A_{ii} = \begin{bmatrix} -\frac{R_{ti}}{L_{ti}} & -\frac{(1-D_i)}{L_{ti}} \\ \frac{(1-D_i)}{C_{ti}} & \sum_{j \in \mathcal{N}_i} -\frac{1}{R_{ij}C_{ti}} \end{bmatrix} \quad (7)$$

The overall global model of the N DGU ImG can be given by,

$$\Sigma_{[N]}^{DGU} : \begin{cases} \dot{\mathbf{x}}(t) = \mathbf{A}\mathbf{x}(t) + \mathbf{B}\mathbf{u}(t) + \mathbf{E}\mathbf{d}(t) \\ \mathbf{y}(t) = \mathbf{C}\mathbf{x}(t) \end{cases} \quad (8)$$

where $\mathbf{x} = (x_{[1]}, x_{[2]}, \dots, x_{[N]}) \in \mathbb{R}^{2N}$, $\mathbf{u} = (u_{[1]}, u_{[2]}, \dots, u_{[N]}) \in \mathbb{R}^N$, $\mathbf{d} = (d_{[1]}, d_{[2]}, \dots, d_{[N]}) \in \mathbb{R}^N$, $\mathbf{y} = (y_{[1]}, y_{[2]}, \dots, y_{[N]}) \in \mathbb{R}^N$. Matrices \mathbf{A} , \mathbf{B} , \mathbf{C} and \mathbf{E} are detailed in the section 6.1 of [44].

2.3 Decentralised Baseline Voltage Control

DeSSf baseline controllers are designed for standalone decoupled converters, assuming a connection to a linear resistive load. As in [44], the baseline controllers are designed for decoupled DGUs using *a priori* knowledge of nominal parameters. In order to track constant voltage references in the presence of constant current disturbances, an integral state error between the reference voltage and output voltage is added to the local DGU model. The dynamics are defined as,

$$\xi_{[i]}(t) = \int_0^t (V_{ref_{[i]}} - y_{[i]}(t)) dt = \int_0^t (V_{ref_{[i]}} - C_i x_{[i]}(t)) dt \quad (9)$$

The DeSSf control law with integral action becomes,

$$\mathcal{C}_{[i]} : u_{[i]}^{bl}(t) = -K_i^{bl} \hat{x}_{[i]}(t) \quad (10)$$

where $K_i^{bl} = [K_i^i, K_i^v, K_i^\xi] \in \mathbb{R}^3$ is the DeSSf control gain vector. Subsequently, the open-loop model augmented with the integral state $\xi_{[i]}(t)$ becomes third order, hence $\bar{x}_{[i]}(t) = [[x_{[i]}(t)]^T, \xi_{[i]}(t)]^T \in \mathbb{R}^3$ is the augmented open-loop state vector. The state-space model of $\Sigma_{[i]}^{DGU}$ can now be defined as,

$$\hat{\Sigma}_{[i]}^{DGU} : \begin{cases} \dot{\bar{x}}_{[i]}(t) = \hat{A}_{ii} \bar{x}_{[i]}(t) + \hat{B}_i u_{[i]}^{bl}(t) + \bar{E}_i \bar{d}_{[i]}(t) + \bar{\zeta}_{[i]}(t) \\ \bar{y}_{[i]}(t) = \bar{C}_i \bar{x}_{[i]}(t) \end{cases} \quad (11)$$

where $\bar{d}_{[i]} = [d_{[i]}, V_{ref_{[i]}}]^T \in \mathbb{R}^2$ is the exogenous signal vector, which includes load current disturbance and reference voltage, $\bar{\zeta}_{[i]}(t) = \sum_{j \in \mathcal{N}_i} \hat{A}_{ij} \bar{x}_{[j]}(t)$, and $\bar{y}_{[i]}(t)$ is the measurable output. $\hat{A}_{ii} \in \mathbb{R}^{3 \times 3}$, $\hat{B}_i \in \mathbb{R}^{3 \times 1}$, $\bar{E}_i \in \mathbb{R}^{3 \times 3}$, $\hat{A}_{ij} \in \mathbb{R}^{3 \times 3}$ and $\bar{C}_i \in \mathbb{R}^3$. $(\hat{A}_{ii}, \hat{B}_i)$ is assumed to be controllable, as demonstrated in [21]. Similarly, the matrices of (11) are defined in [44]. The DeSSf controllers can be tuned via pole placement or using linear quadratic integral (LQI) regulation.

3 Distributed \mathcal{L}_1 Adaptive Control Architecture

The \mathcal{L}_1 AC is a modification of the indirect MRAC architecture and was developed to address the issues of providing transient guarantees and determining an optimal rate of adaptation without sacrificing robustness to uncertainty [34]. Conventional MRAC suffers from a trade-off between estimation and robustness; large adaptive gains induce high gain feedback which usually leads to high-frequency oscillations in the control-channel that can destabilise the control-loop. The \mathcal{L}_1 AC architecture decouples the trade-off between estimation and robustness by inserting a low-pass filter (LPF) at the input to both the plant and state-predictor, as seen in Fig. 2. Consequently, robustness instead depends on the choice of filter-bandwidth rather than the adaptive gain, thus allowing fast adaptation. Performance bounds and asymptotic stability are derived using Lyapunov based methods. The \mathcal{L}_1 AC has achieved successful implementations in various

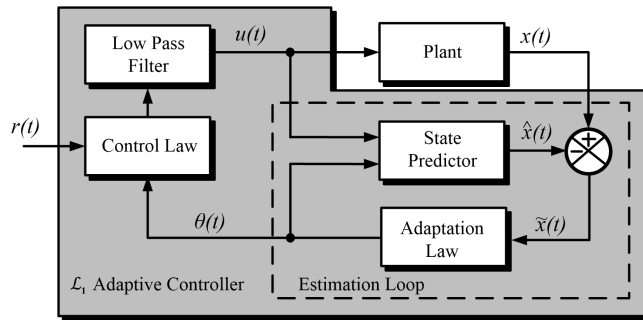


Figure 2: General Architecture of \mathcal{L}_1 Adaptive Controller. Adapted from [34]

safety-critical applications; notably in aircraft auto-pilots, where the \mathcal{L}_1 AC is used to maintain stability and good performance in conditions of high aerodynamic uncertainty, and during faults such as, component failure and communication latencies [38]. Other \mathcal{L}_1 AC applications include unmanned water [39] and aerial vehicles [37]. These applications require controllers that can maintain safe and reliable operation across large operating ranges that experience uncertain conditions. The \mathcal{L}_1 AC achieves scalable behaviour across different speed ranges, operating dynamics (e.g. surge/cruise), payload and vehicle sizes. Furthermore, \mathcal{L}_1 AC has been used to augment an LQR baseline controller to enhance the performance tracking enhancement of a decentralised leader-follower coordination scheme for unmanned aerial vehicles [42]. While receiving great attention in aerospace applications, there are many attractive opportunities for the \mathcal{L}_1 AC architecture in smart-grid applications. Recently, the \mathcal{L}_1 AC has been implemented to achieve robust maximum power-point tracking of a wind turbine during uncertainty conditions such as shadow effects, wind shear and speed variations [41]. Ultimately, the \mathcal{L}_1 AC architecture has potential to improve mG voltage control in heterogeneous and uncertain environments.

From Fig. 2 a state-predictor replaces the reference model of the conventional MRAC, and a LPF limits the control signal bandwidth. The state-error dynamics, $\tilde{x}(t)$, between the plant and state-predictor drives the adaptation law. This adjusts the control parameters in order to ensure bounded and asymptotic convergence of state and estimation signals.

3.1 Plant structure

The plant has a known structure, but with unknown parameter values.

Assumption 2: *The design of the distributed \mathcal{L}_1 AC architecture can neglect the exogenous load disturbance signal $d_{[i]}(t)$ as it is compensated by the integral action of $u_{[i]}^{bl}(t)$.*

A matched uncertainty term is introduced to represent parametric uncertainty in the dynamics of

$\hat{\Sigma}_{[i]}^{\text{DGU}}$, hence (11) can be represented as,

$$\hat{\Sigma}_{[i]}^{\text{DGU}} : \begin{cases} \dot{\bar{x}}_{[i]}(t) = \hat{A}_{ii}\bar{x}_{[i]}(t) + \hat{B}_i(u_{[i]}(t) + \theta_{[i]}(t)\hat{x}_{[i]}(t)) + F\bar{E}_i\bar{d}_{[i]}(t) + \bar{\zeta}_{[i]}(t) \\ \bar{y}_{[i]}(t) = \bar{C}_i\bar{x}_{[i]}(t) \end{cases} \quad (12)$$

where $\bar{x}_{[i]}(t) \in \mathbb{R}^3$, is the system measurable state vector; $u(t) \in \mathbb{R}$ is the control signal; $F = [0, 0, 1]$; $\theta_{[i]}(t)$ is the unknown matched parametric uncertainty vector. This belongs to a known compact convex set of uniform boundedness $\theta \in \Theta \subset \mathbb{R}^3$.

3.2 Control Law

The small-signal control input $u(t)$ for $\hat{\Sigma}_{[i]}^{\text{DGU}}$ consists of the summation between the baseline and $\mathcal{L}_1\text{AC}$ control signals,

$$\mathcal{L}_{[i]}^{\mathcal{L}_1} : u_{[i]}(t) = u_{[i]}^{bl}(t) + u_{[i]}^{\mathcal{L}_1}(t) \quad (13)$$

The Laplace domain representation of the augmenting $\mathcal{L}_1\text{AC}$ law, fitted with a first-order LPF, is

$$u_{[i]}^{\mathcal{L}_1}(s) = -C(s)[\hat{\theta}_{[i]}\hat{x}_{[i]}](t) \quad (14)$$

where $C(s) = \frac{\omega_c}{s + \omega_c}$, $\hat{\theta} \in \mathbb{R}^3$ is the parametric estimation vector. The robustness of the $\mathcal{L}_1\text{AC}$ is dependent on the LPF bandwidth ω_c , as subsequently designed.

3.3 State-Predictor

Remark 1. *Following section 3.1.3 of [44], as the parameters of \bar{B}_i are unknown, the state-predictor dynamics are defined in control canonical form. For readability, we keep state notation in terms of $x_{[i]}(t)$ as opposed to $z_{[i]}(t)$ in [44].*

The state-predictor generates an estimate of the system states. From the perspective of the $\mathcal{L}_1\text{AC}$, the baseline dynamics are combined with the open-loop DGU dynamics to form an augmented closed-loop system. As the design of the $\mathcal{L}_1\text{AC}$ is distributed, the structure of the state-predictor requires measurement of neighbouring predictor states. The reasoning becomes apparent when guaranteeing GAS. Without loss of generality, the state-predictor formulation and the desired closed-loop dynamics are equal for all DGUs,

$$\mathcal{E}_{[i]} : \begin{cases} \dot{\hat{x}}_{[i]}(t) = \hat{A}_m\hat{x}_{[i]}(t) + b(u_{[i]}^{\mathcal{L}_1}(t) + \hat{\theta}_{[i]}(t)\hat{x}_{[i]}(t)) + F\hat{E}_i\hat{d}_{[i]}(t) + \hat{\zeta}_{[i]}(t) \\ \hat{y}_{[i]}(t) = \hat{C}_i\hat{x}_{[i]}(t) \end{cases} \quad (15)$$

where $\hat{A}_m \in \mathbb{R}^{3 \times 3}$ is the Hurwitz design matrix that specifies the desired closed-loop dynamics and b is the input vector in control canonical form of [44].

3.4 Local Adaptive Law and Global Asymptotic Stability

The adaptive law of local $\mathcal{L}_1\text{AC}$ s generates an estimate of the uncertainties that each DGU experiences, such as unknown parameters, change in dynamics due to PnP operations, topology change, unexpected disturbances and possible faults. Ensuring stable adaptation and bounded signals is based on Lyapunov's second method of stability. By defining the Lyapunov function in terms of local state-error and parametric estimation error vectors, the energy trajectories of local system states and estimates remain bounded and local asymptotic stability is guaranteed. Moreover, this paper structures the Lyapunov function as an ARE, the solution of which guarantees GAS, as in [45–47]. Local state error is defined as, $\tilde{x}_{[i]}(t) = \bar{x}_{[i]}(t) - \hat{x}_{[i]}(t) \in \mathbb{R}^3$ in control canonical

form. The estimate error is defined as $\tilde{\theta}_{[i]}(t) = \bar{\theta}_{[i]}(t) - \hat{\theta}_{[i]}(t) \in \mathbb{R}^3$. The state-error dynamics, used to drive the adaptive law, is defined as,

$$\dot{\tilde{x}}_{[i]}(t) = \hat{A}_m \tilde{x}_{[i]}(t) + b\tilde{\theta}(t)\tilde{x}_{[i]}(t) + \sum_{j \in \mathcal{N}_i} \hat{A}_{ij} \tilde{x}_{[j]}(t) \quad (16)$$

The quadratic Lyapunov function candidate that describes the aggregated global energy within the system is defined as,

$$\mathcal{V}(\tilde{x}(t), \tilde{\theta}(t)) = \sum_{i=0}^N (\tilde{x}_{[i]}(t)^T P_i \tilde{x}_{[i]}(t) + \tilde{\theta}_{[i]}(t)^T \Gamma_i^{-1} \tilde{\theta}_{[i]}(t)) \quad (17)$$

where, $P_i \in \mathbb{R}^{3 \times 3}$ is a symmetric matrix, such that $P_i = P_i^T > 0$ is the solution to the Lyapunov linear inequality $\hat{A}_m^T P_i + P_i \hat{A}_m \leq -Q_i$, for arbitrary $Q_i = Q_i^T > 0$, and $\Gamma_i \in \mathbb{R}^+$ is the adaptive gain. The derivative of (17) can be written as,

$$\dot{\mathcal{V}}(t) \leq \sum_{i=0}^N (2(\hat{A}_m \tilde{x}_{[i]} + b\tilde{\theta}_{[i]} \hat{x}_{[i]} + \sum_{j \in \mathcal{N}_i} A_{ij} \tilde{x}_{[j]}) P_i \tilde{x}_{[i]} + \tilde{\theta}_{[i]} \Gamma_i^{-1} \dot{\tilde{\theta}}_{[i]}) \quad (18)$$

The adaptive law for the uncertainty estimate is given as,

$$\dot{\hat{\theta}}_{[i]} = \Gamma_i \text{Proj}(\hat{\theta}_{[i]}, -x_{[i]}(t)\tilde{x}_{[i]}^T(t)P_i b) \quad (19)$$

The projection operator, described in [34], is used to prevent parametric drift by upper-bounding the parameter estimate *a priori* i.e. θ_{max} . This, along with the LPF, allows for robust-adaptation. With this, (18) becomes,

$$\dot{\mathcal{V}}(t) = \sum_{i \leq 0}^N (\tilde{x}_{[i]}^T (\hat{A}_m^T P_i + P_i \hat{A}_m) \tilde{x}_{[i]} + P_i \tilde{x}_{[i]}^T \sum_{j \in \mathcal{N}_i} A_{ij} \tilde{x}_{[j]} + (\sum_{j \in \mathcal{N}_i} A_{ij} \tilde{x}_{[j]}) P_i \tilde{x}_{[i]}) \quad (20)$$

Expanding the two summation terms of (20) and using the inequality $X^T Y + Y^T X \leq X^T X + Y^T Y$ from [45] yields,

$$\dot{\mathcal{V}}_{[i]}(t) \leq \sum_{i=0}^N (\tilde{x}_{[i]}^T (\hat{A}_m^T P_i + P_i \hat{A}_m) \tilde{x}_{[i]} + N_i \tilde{x}_{[i]}^T (P_i^T P_i) \tilde{x}_{[i]} + \sum_{j \in \mathcal{N}_i} \tilde{x}_{[j]}^T (A_{ij}^T A_{ij}) \tilde{x}_{[j]}) \quad (21)$$

Assumption 3: For conservativeness, knowledge of the upper-bound on the coupling gain matrix \hat{A}_{ij} is assumed for all DGUs.

The coupling term in (21) can be upper bounded as,

$$\sum_{j \in \mathcal{N}_i} \tilde{x}_{[j]}^T (\hat{A}_{ij}^T \hat{A}_{ij}) \tilde{x}_{[j]} \leq \Xi_i^2 \sum_{j \in \mathcal{N}_i} \tilde{x}_{[j]}^T \tilde{x}_{[j]} \quad (22)$$

where $\Xi_i^2 \triangleq \sum_{j \in \mathcal{N}_i} \lambda_{max}(\hat{A}_{ij}^T \hat{A}_{ij}) = \sum_{j \in \mathcal{N}_i} \lambda_{max}(\hat{A}_{ij}^2) \leq N_i \lambda_{max}(\hat{A}_{ij}^2)$, and λ_{max} corresponds to the maximum eigenvalue. Finally, following some index manipulation in [44],

$$\dot{\mathcal{V}}(t) \leq \sum_{i=0}^N \tilde{x}_{[i]}^T (A_m^T P_i + P_i A_m + N_i P_i P_i + \Xi_i^2 \mathbb{I}) \tilde{x}_{[i]} \quad (23)$$

The global vector Lyapunov function is structured as an ARE such that if there exists a positive-definite matrix P_i that solves each local ARE $A_m^T P_i + P_i A_m + N_i P_i P_i + (\Xi_i^2 + \epsilon_i) \mathbb{I} = 0$, where $\epsilon_i > 0$, then

$$\dot{\mathcal{V}}(t) \leq - \sum_{i=0}^N \tilde{x}_{[i]}^T \epsilon_{[i]} \tilde{x}_{[i]} \quad (24)$$

To ensure a positive-definite P_i exists for each $\mathcal{L}_1\text{AC}$, Lemma's 1 and 2 from [47] are invoked. Lemma 1 states that the Hamiltonian matrix associated with the ARE must be hyperbolic for $P_i > 0$ to exist. Lemma 2 states that for such a Hamiltonian matrix to be hyperbolic, the following condition must be satisfied,

$$\gamma \triangleq \min_{\omega \in \mathbb{R}^+} \sigma_{\min}(A_m - j\omega\mathbb{I}) > \sqrt{N_i \Xi_i^2} > 0 \quad (25)$$

Therefore, the desired closed-loop dynamics should be designed such that the distance between desired eigenvalues and the imaginary axis is greater than $\sqrt{N_i \Xi_i^2}$. To compute the distance γ , the bisection method of [49], shown in section of 7.5 of [47], is used. Furthermore, Barbalat's Lemma can be invoked to show that global system states converge to the desired states i.e. $\lim_{t \rightarrow \infty} \tilde{x}_{[i]}(t) = 0$. Ultimately, GAS of the overall adaptive DC ImG is guaranteed when the adaptive law is chosen as in (19) and the design condition (25) is satisfied.

3.5 Filter Design

The key feature of the $\mathcal{L}_1\text{AC}$ architecture is the design of a LPF which decouples robustness from adaptation. At this point, GAS has been guaranteed during nominal operation and adaptation. Here, boundedness and stability is further guaranteed when the LPF is inserted. The LPF bandwidth is tuned using the \mathcal{L}_1 norm condition. A reference system is defined for the predictor in order to facilitate performance specification in the Laplace domain. $\hat{\theta}_{[i]}(t) \rightarrow \theta_{[i]}$ is assumed.

$$\hat{x}_{ref[i]}(s) = (s\mathbb{I} - \hat{A}_m)^{-1}b((1 - C(s))\theta_{[i]}(\hat{x}_{ref[i]}(t) + \tilde{x}_{[i]}(t)) + F\hat{d}_{[i]}(s) + \hat{\zeta}_{[i]}(s) + \hat{x}_{ic[i]}(s) \quad (26)$$

where $\hat{x}_{ref[i]} \in \mathbb{R}^3$, is the reference state vector, $\hat{x}_{ic[i]} \in \mathbb{R}^3$ is the initial state vector, $\mathbb{I} \in \mathbb{R}^{3 \times 3}$, is the identity matrix. From (24), $\tilde{x}_{[i]}(t)$ is bounded, and $\theta_{[i]}$ is bounded by θ_{max} , which represents the boundary of adaptation. Initial states can be assumed bounded, while the reference signal vector $F\hat{d}_{[i]}(t)$ is a constant. To ensure the local reference states remain bounded when the LPF is inserted, a sufficient stability condition via the small-gain theorem is,

$$\lambda = \|G(s)\|_{\mathcal{L}_1} \theta_{max} < 1 \quad (27)$$

where, the desired local closed-loop behaviour is represented by the transfer function, $H(s) = (s\mathbb{I} - \hat{A}_m)^{-1}b$ and $G(s) = H(s)(1 - C(s))$. The adaptation bound is defined as,

$$\theta_{max} = \max_{\theta \in \Theta} \|\theta\|_1 \quad (28)$$

The states of the overall reference system are bounded if the interconnection term $\hat{\zeta}_{[i]}(t)$ remains bounded. The interconnection term, $\hat{\zeta}_{[i]}(t) \leq N_i \lambda_{max}(\hat{A}_{ij})x_{ref[j]}(s)$, is bounded if (27) is also satisfied for $\mathcal{E}_{[j]}$ since condition (27) applies for all DGUs.

3.6 Algorithm for Controller Design

Algorithm 1 collects the steps of the overall design procedure.

Algorithm 1 Design of distributed controllers $\mathcal{C}_{[i]}^{\mathcal{L}_1}$ for subsystem $\hat{\Sigma}_{[i]}^{\text{DGU}}$

Input: $\mathcal{E}_{[i]}$ as in (15), \mathcal{N}_i , Ξ_i^2 , θ_{max}

Output: Controller $\mathcal{C}_{[i]}^{\mathcal{L}_1}$ as in (4.4)

(I) Design \hat{A}_m , as in [44], such that (25) is satisfied. Find P_i , the solution to the ARE of (23).

(II) Select ω_c , such that (27) is satisfied.

The overall distributed architecture is shown in Fig. 3.

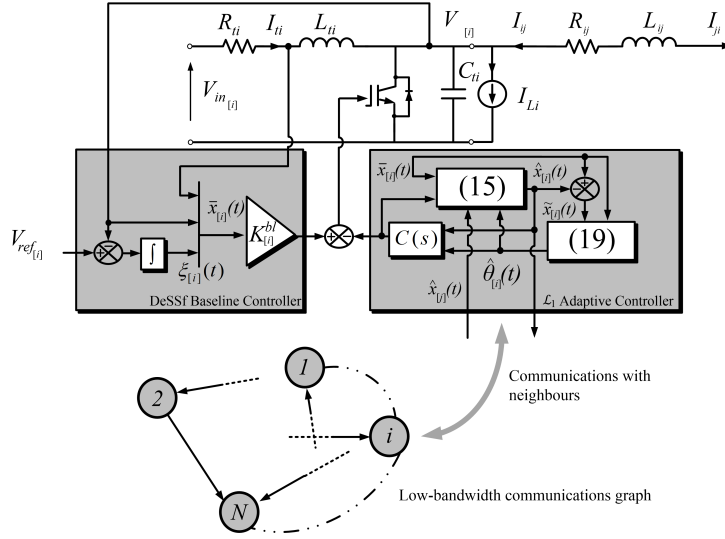


Figure 3: Overall Distributed Control Architecture of $\hat{\Sigma}_{[i]}^{\text{DGU}}$.

4 Results

A meshed and radial mG topology, similar to that of [21], is considered in this work. Equipped with only baseline controllers, this system is known to destabilise when $\hat{\Sigma}_{[6]}^{\text{DGU}}$ is plugged-in. Hence, this set-up can adequately evaluate the performance of the proposed distributed $\mathcal{L}_1\text{AC}$ architecture. Each DGU is equipped with controllers $\mathcal{C}_{[i]}^{\mathcal{L}_1}$, $i = 1, \dots, 6$.

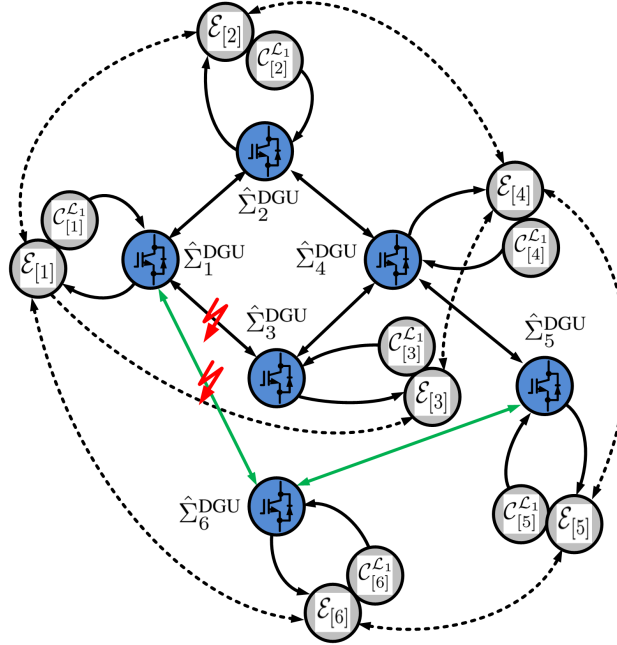


Figure 4: Islanded-microgrid configuration with communications graph (dotted) - $\hat{\Sigma}_{[6]}^{\text{DGU}}$ plug-in (green), and topology change (red).

Simulations are performed in Matlab/Simulink using the simpowersystems toolbox. While the averaged model of the ImG is used in [44], this paper uses the non-linear switching model for

greater authenticity. System parameters are detailed in Table 1.

Table 1: System Parameters

Description	Parameter	$\hat{\Sigma}_1^{\text{DGU}}$	$\hat{\Sigma}_2^{\text{DGU}}$	$\hat{\Sigma}_3^{\text{DGU}}$	$\hat{\Sigma}_4^{\text{DGU}}$	$\hat{\Sigma}_5^{\text{DGU}}$	$\hat{\Sigma}_6^{\text{DGU}}$
DGU rated power (kW)	$P_{[i]}$	5	5	5	5	5	5
Local load demand (kW)	$P_{R[i]}$	2.5	2	1.8	2.5	3	2.5
Input voltage (V)	$V_{in[i]}$	95	100	90	105	92	90
Reference voltage (V)	$V_{ref[i]}$	381	380.5	380.2	379	379.5	380.7
Switching frequency (kHz)	f_s	25	25	25	25	25	25
Duty cycle	D_i	0.7507	0.7372	0.7633	0.723	0.7576	0.7636
Inductance (μH)	L_{ti}	28.47	89.62	192.5	70	35	93.34
Capacitance (μF)	C_{ti}	37.632	51.67	40.73	37	31	24.66
Parasitic resistance (Ω)	R_{ti}	0.02	0.04	0.02	0.2	0.4	0.5
Line resistance (Ω)	R_{ij}	0.5-2-10	0.5-4	2-4	2-4-15	15-4	10-4
Line inductance (μH)	L_{ij}	10-70-800	40-70	70-70	70-70-25	25-90	800-90
Nominal duty cycle	D_i	0.7368	0.7368	0.7368	0.723	0.7368	0.7368
Nominal inductance (μH)	L_{tnom}	2.794	2.794	2.794	2.794	2.794	2.794
Nominal capacitance (μF)	C_{tnom}	60.6	60.6	60.6	60.6	60.6	60.6
Nominal parasitic resistance (Ω)	R_{tnom}	0.1	0.1	0.1	0.1	0.1	0.1
Nominal line resistance (Ω)	R_{ijnom}	1	1	1	1	1	1
Nominal line inductance (μH)	L_{ijnom}	10	10	10	10	10	10

The dynamics of each DGU are different i.e. the electrical parameters and controller bandwidths are non-identical; therefore, the system can be defined as heterogeneous. The tests include PnP operations, robustness to topology change and unknown load disturbances, and output voltage reference tracking. The architecture is also evaluated using a bus-connected topology.

4.1 Plug-and-play operations

At $t = 0.05$ s, $\hat{\Sigma}_{[6]}^{\text{DGU}}$ is plugged-in to the network. Fig. 5(a) shows that $\hat{\Sigma}_{[6]}^{\text{DGU}}$ seamlessly plugs-in and remains stable thereafter.

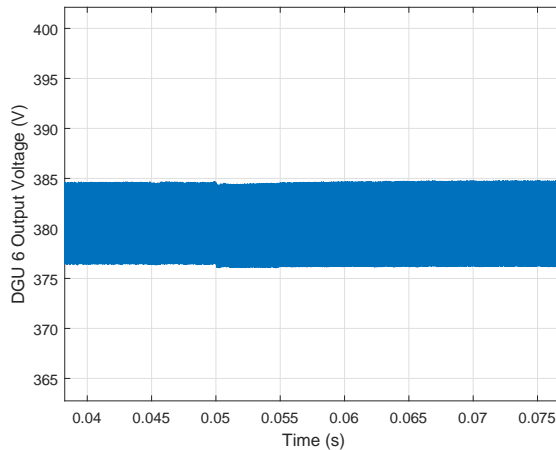


Figure 5: $\hat{\Sigma}_{[6]}^{\text{DGU}}$ voltage response during plug-in.

At $t = 0.15$ s, lines connecting $\hat{\Sigma}_{[1]}^{\text{DGU}}$ to $\hat{\Sigma}_{[3]}^{\text{DGU}}$ and $\hat{\Sigma}_{[6]}^{\text{DGU}}$ are disconnected due to a fault. Thus, the topology of the ImG changes; it is no longer radial. Fig. 6 shows $\hat{\Sigma}_{[1]}^{\text{DGU}}$ has fast and robust behaviour; after a 1 V overshoot, the response settles within 5 ms.

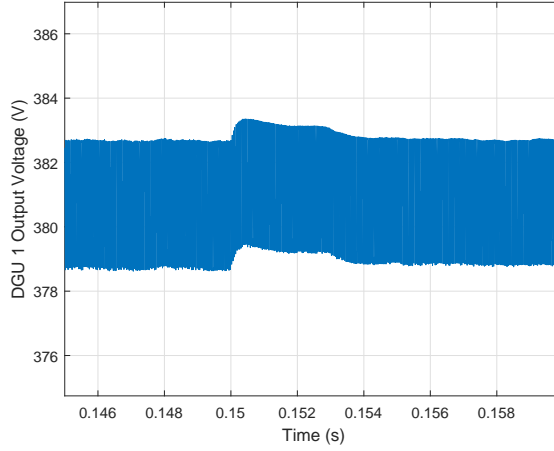


Figure 6: $\hat{\Sigma}_{[1]}^{\text{DGU}}$ during topology change.

4.2 Robustness to unknown load changes

Robustness to an unknown load change is evaluated by stepping the load power of $\hat{\Sigma}_{[6]}^{\text{DGU}}$ at $t = 0.3$ s from 2.5 kW to 800 W. Fig. 7 shows that though overshoot amounts to 7.8 %, settling is achieved within 30 ms.

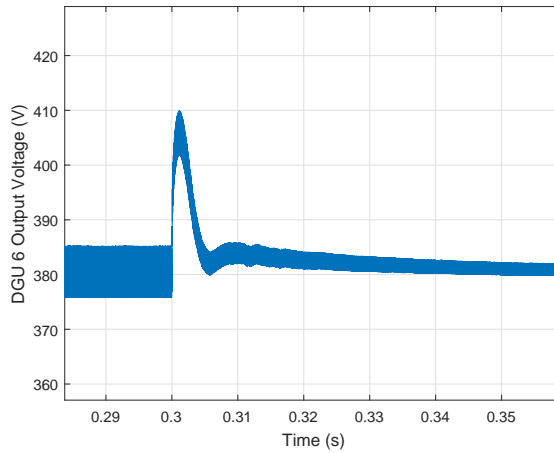


Figure 7: $\hat{\Sigma}_{[6]}^{\text{DGU}}$ voltage response for 2.5 kW - 800 W load change.

4.3 Output voltage reference tracking

The hierarchical structure of mG control structures requires primary level reference changes. Commands are sent from secondary controllers, in order to control the power flows amongst DGUs within the mG, as well as regulate the state-of-charge of batteries. Therefore, a key metric of the proposed system is the performance of the system in response to voltage reference changes. This is evaluated by stepping the voltage reference of $\hat{\Sigma}_{[5]}^{\text{DGU}}$ from 379.5 V to 377 V.

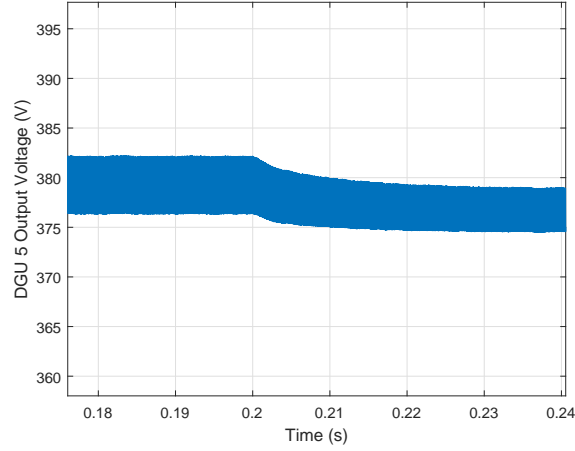


Figure 8: $\hat{\Sigma}_{[5]}^{\text{DGU}}$ voltage reference step change of 379 V - 377 V.

4.4 Bus-connected topology

A bus-connected topology is used to highlight the flexibility of designing controls for arbitrary topologies.

Remark 2. *Since typical mG loads are not directly connected to each DGU i.e. bus-connected topology, Kron reduction analysis is required to transpose the coupling parameters of the bus-connected into those of the load-connected topology of Fig. 1 that the design is based on. The advantage of the proposed adaptive design over state-of-the-art PnP techniques is that robustness to the change of parameter values can be incorporated.*

Fig. 9 shows a typical bus-connected topology.

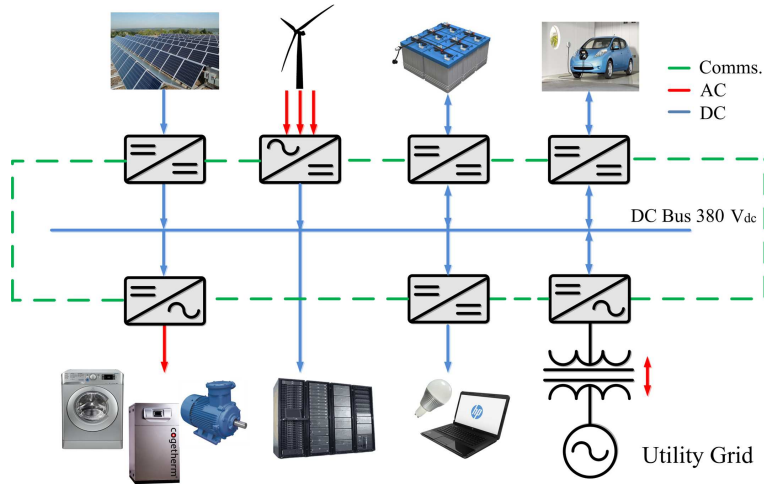
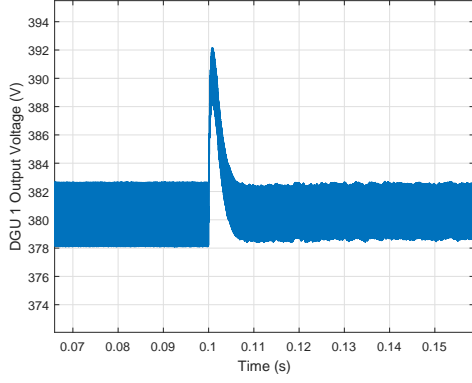
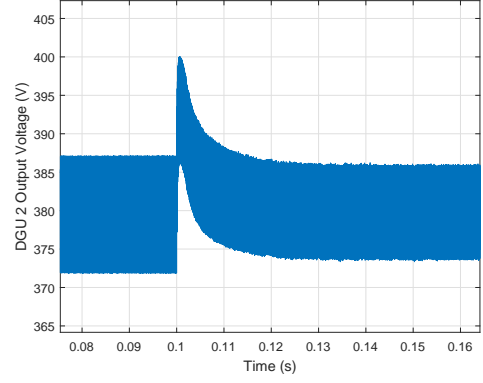


Figure 9: Typical bus-connected topology, adapted from [50].

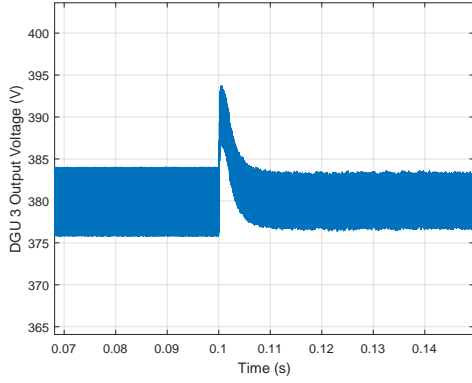
Following [15], in which a resistive load of 15 kW and a 3.8 kW closed-loop speed controlled DC motor are connected to the 380 V bus, and powered by 2 DGUs, we implement the same but with 6 DGUs connected. Fig. 10(f) shows the response of $\hat{\Sigma}_{[6]}^{\text{DGU}}$ plugging-in at $t = 0.1$ s. Stability is maintained during PnP operations and responses settle within 20 ms.



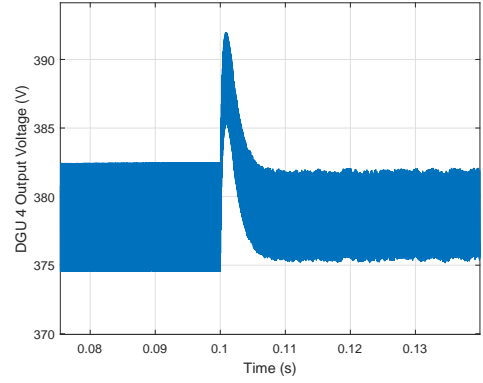
(a) $\hat{\Sigma}_1^{\text{DGU}}$ output voltage



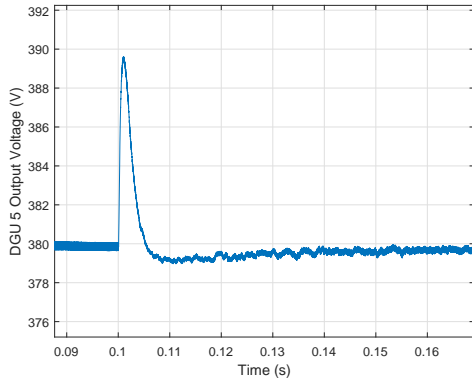
(b) $\hat{\Sigma}_2^{\text{DGU}}$ output voltage



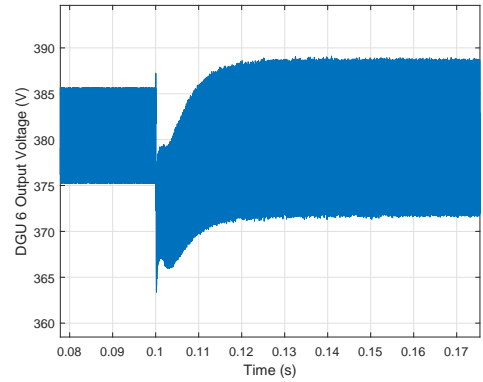
(c) $\hat{\Sigma}_3^{\text{DGU}}$ output voltage



(d) $\hat{\Sigma}_4^{\text{DGU}}$ output voltage



(e) $\hat{\Sigma}_5^{\text{DGU}}$ output voltage

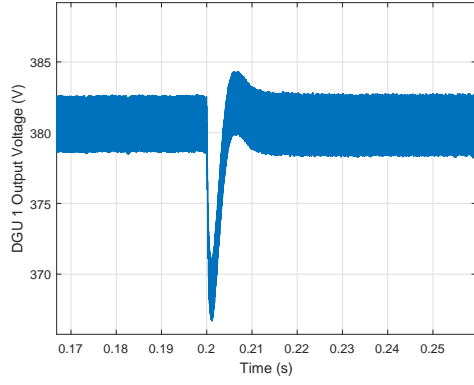


(f) $\hat{\Sigma}_6^{\text{DGU}}$ output voltage

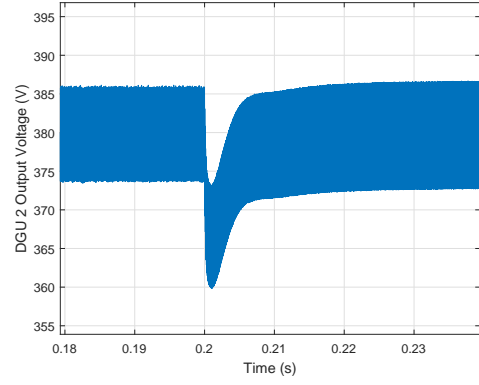
Figure 10: DGU output voltage responses in bus-connected topology to $\hat{\Sigma}_{[6]}^{\text{DGU}}$ plug-in.

At $t = 0.2$ s, $\hat{\Sigma}_{[3]}^{\text{DGU}}$ is plugged-out. Fig. 11 plots the responses of all the DGUs.

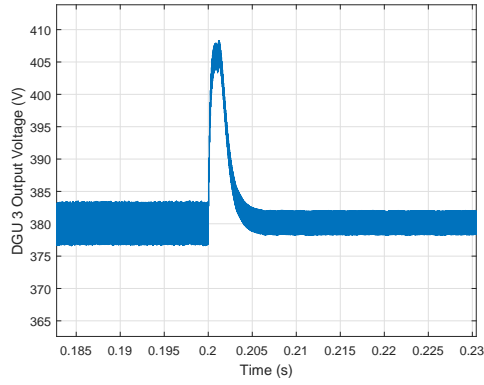
Again, stability is maintained, with the worst case response associated with $\hat{\Sigma}_5^{\text{DGU}}$ in Fig. 11(e) which shows a settling time of nearly 30 ms and $\hat{\Sigma}_6^{\text{DGU}}$ in Fig. 11(f).



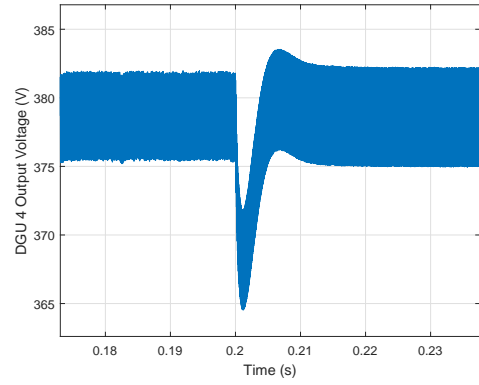
(a) $\hat{\Sigma}_1^{\text{DGU}}$ output voltage



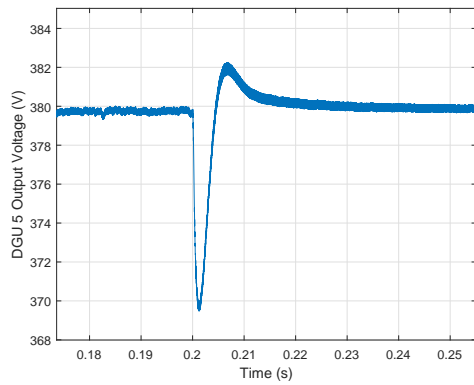
(b) $\hat{\Sigma}_2^{\text{DGU}}$ output voltage



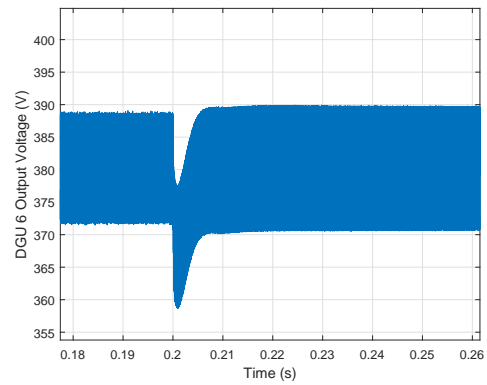
(c) $\hat{\Sigma}_3^{\text{DGU}}$ output voltage



(d) $\hat{\Sigma}_4^{\text{DGU}}$ output voltage



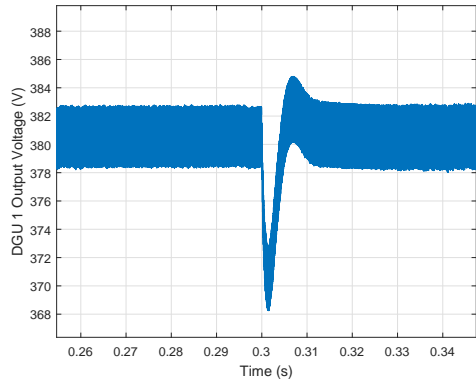
(e) $\hat{\Sigma}_5^{\text{DGU}}$ output voltage



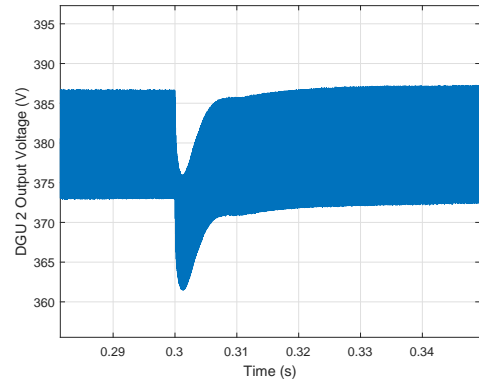
(f) $\hat{\Sigma}_6^{\text{DGU}}$ output voltage

Figure 11: DGU output voltage responses to $\hat{\Sigma}_{[3]}^{\text{DGU}}$ plug-out in bus-connected topology.

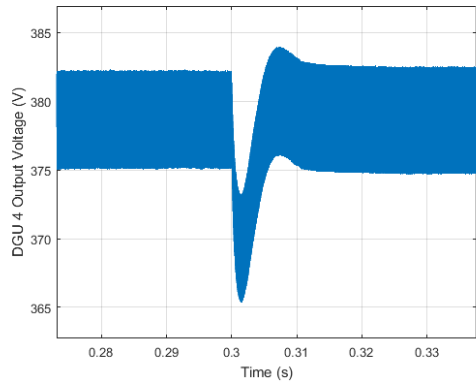
Finally, the resistive load power is changed from 15 kW to 18 kW.



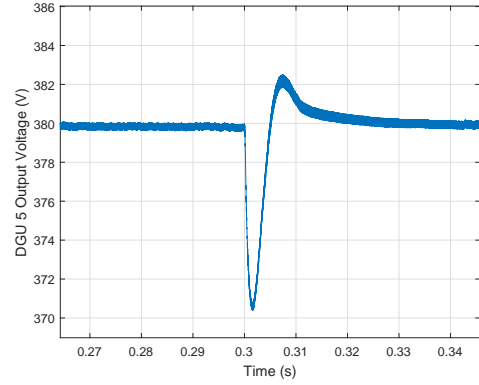
(a) $\hat{\Sigma}_{[1]}^{\text{DGU}}$ output voltage.



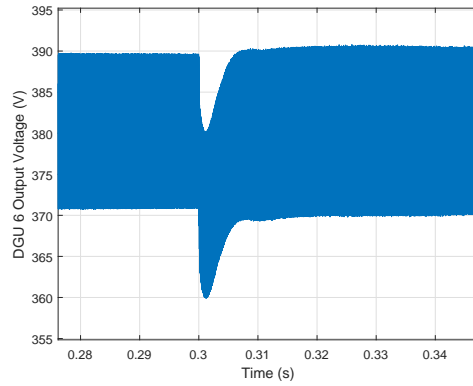
(b) $\hat{\Sigma}_{[2]}^{\text{DGU}}$ output voltage.



(c) $\hat{\Sigma}_{[4]}^{\text{DGU}}$ output voltage.



(d) $\hat{\Sigma}_{[5]}^{\text{DGU}}$ output voltage.



(e) $\hat{\Sigma}_{[6]}^{\text{DGU}}$ output voltage

Figure 12: DGU output voltage responses to 15 kW - 18 kW load step change in bus-connected topology.

Fig. 12(e) shows the response of $\hat{\Sigma}_{[6]}^{\text{DGU}}$ settling within 15 ms.

5 Conclusion

This paper develops a novel scalable distributed \mathcal{L}_1 AC architecture for the primary voltage control level of large-scale DC ImGs with arbitrary topology. \mathcal{L}_1 adaptive controllers were designed with self-commissioning capabilities in that existing baseline controllers can be augmented and GAS is guaranteed in a plug-and-play fashion. The distributed architecture is shown to ensure GAS in the presence of large-gain interconnections and parametric, topology, and PnP operation uncertainty. This requires knowledge of the upper-bound on interconnection terms and measurement of neighbouring predictor states in order to solve local AREs.

The architecture was successfully evaluated using a heterogeneous radial and meshed ImG that consisted of DC-DC boost converters. Fast and robust voltage control is achieved during PnP operations, topology changes and unknown load disturbances. The flexibility of the control orientated design approach was evaluated using a bus-connected topology consisting of resistive and closed-loop controlled DC motor loads. Kron reduction analysis, typically required by state-of-the-art PnP techniques, can be relaxed due to the adaptive nature of the controller. Ultimately, with the presence of LBC in the conventional secondary and tertiary levels of the mG control hierarchy, a distributed primary control architecture is feasible.

Future work will continue to investigate cases of robustness as further conditions are required for coupling-independence, and for the architecture to provide stability in mGs with constant-power loads. Moreover, the proposed architecture will be designed with purely adaptive controllers, implemented for current controls and evaluated when equipped with secondary/coordination control layers.

References

- [1] R. W. De Doncker, "Power electronic technologies for flexible DC distribution grids," in *Power Electronics Conference (IPEC-Hiroshima 2014-ECCE-ASIA), 2014 International. IEEE, 2014*, 2014, pp. 736–743.
- [2] D. P. Symanski, "Residential & Commercial Use Of DC Power," in *UL & NFPA-Low Voltage Direct Current Workshop*. Arlington, Virginia: EPRI, 2011.
- [3] B. T. Patterson, "DC, Come Home: DC Microgrids and the Birth of the "Enernet",," *IEEE Power and Energy Mag.*, vol. 10, no. 6, pp. 60–69, 2012.
- [4] D. J. Becker and B. J. Sonnenberg, "DC microgrids in buildings and data centers," in *Telecom. Energy Conference (INTELEC)*, 2011.
- [5] A. T. Elsayed, A. A. Mohamed, and O. A. Mohammed, "DC microgrids and distribution systems: An overview," *Electric Power Systems Research*, vol. 119, pp. 407–417, 2015.
- [6] E. R. Diaz, X. Su, M. Savaghebi, J. C. Vasquez, M. Han, and J. M. Guerrero, "Intelligent DC microgrid living laboratories - A Chinese-danish cooperation project," *2015 IEEE 1st International Conference on Direct Current Microgrids, ICDCM 2015*, pp. 365–370, 2015.
- [7] a. a. Abdelhafez and a. J. Forsyth, "A Review of More-Electric Aircraft," *Aerospace Sciences & Aviation Technology*, pp. 1–13, 2009.
- [8] P. Wheeler and S. Bozhko, "The more electric aircraft: Technology and challenges," *IEEE Electrification Magazine*, vol. 2, no. 4, pp. 6–12, 2014.
- [9] D. E. Olivares, A. Mehrizi-Sani, A. H. Etemadi, C. A. Cañizares, R. Iravani, M. Kazerani, A. H. Hajimiragha, O. Gomis-Bellmunt, M. Saeedifard, R. Palma-Behnke, G. A. Jiménez-Estévez, and N. D. Hatziargyriou, "Trends in microgrid control," *IEEE Transactions on Smart Grid*, vol. 5, no. 4, pp. 1905–1919, 2014.

- [10] M. A. Anuradha and A. Massoud, *IEEE Vision for Smart Grid Controls: 2030 and Beyond: Roadmap*. IEEE CSS, 2013.
- [11] S. Rivero, “Distributed & Plug-and-Play Control For Constrained Systems,” Ph.D. dissertation, 2013.
- [12] N. L. Diaz, T. Dragicevic, J. C. Vasquez, and J. M. Guerrero, “Intelligent distributed generation and storage units for DC microgrids - A new concept on cooperative control without communications beyond droop control,” *IEEE Transactions on Smart Grid*, vol. 5, no. 5, pp. 2476–2485, sep 2014.
- [13] M. Kumar, S. C. Srivastava, and S. N. Singh, “Control Strategies of a DC Microgrid for Grid Connected and Islanded Operations,” *IEEE Transactions on Smart Grid*, vol. 6, no. 4, pp. 1588–1601, 2015.
- [14] D. Wu, F. Tang, T. Dragicevic, J. M. Guerrero, and J. C. Vasquez, “Coordinated control based on bus-signaling and virtual inertia for Islanded DC Microgrids,” *IEEE Transactions on Smart Grid*, vol. 6, no. 6, pp. 2627–2638, nov 2015.
- [15] D. O’Keeffe, S. Rivero, L. Albiol-Tendillo, and G. Lightbody, “Distributed Hierarchical Droop Control of Boost Converters in DC Microgrids,” *28th IEEE Irish Signals and Systems Conference*, pp. 1–6, 2017.
- [16] L. Meng, Q. Shafiee, G. F. Trecate, H. Karimi, D. Fulwani, X. Lu, and J. M. Guerrero, “Review on Control of DC Microgrids and Multiple Microgrid Clusters,” *IEEE Journal of Emerging and Selected Topics in Power Electronics*, vol. 5, no. 3, pp. 928–948, 2017.
- [17] F. Katiraei, A. Zamani, and R. Masiello, “Microgrid Control Systems,” *IEEE Power and Energy Magazine*, vol. 15, no. 4, pp. 116–112, 2017.
- [18] J. Å. Stoustrup, “Plug & Play Control : Control Technology Towards New Challenges,” *European Journal of Control*, vol. 15, no. 3-4, pp. 311–330, 2009.
- [19] S. Rivero, F. Sarzo, and G. Ferrari-Trecate, “Plug-and-Play Voltage and Frequency Control of Islanded Microgrids with Meshed Topology,” *IEEE Transactions on Smart Grid*, vol. 6, no. 3, pp. 1176–1184, 2015.
- [20] S. Rivero, M. Tucci, J. C. Vasquez, J. M. Guerrero, and G. Ferrari-Trecate, “Stabilizing plug-and-play regulators and secondary coordinated control for AC islanded microgrids with bus-connected topology,” *Applied Energy*, no. August, pp. 1–21, 2017.
- [21] M. Tucci, S. Rivero, J. C. Vasquez, J. M. Guerrero, and G. Ferrari-Trecate, “A Decentralized Scalable Approach to Voltage Control of DC Islanded Microgrids,” *IEEE Transactions on Control Systems Technology*, vol. 24, no. 6, pp. 1965–1979, 2016.
- [22] M. Tucci, L. Meng, J. M. Guerrero, and G. Ferrari-Trecate, “Plug-and-play control and consensus algorithms for current sharing in DC microgrids,” in *IFAC-PapersOnLine*, vol. 50, 2016, pp. 1–23.
- [23] R. Han, M. Tucci, R. Soloperto, A. Martinelli, G. Ferrari-Trecate, and J. M. Guerrero, “Hierarchical Plug-and-Play Voltage/Current Controller of DC microgrid with Grid-Forming/Feeding modules: Line-independent Primary Stabilization and Leader-based Distributed Secondary Regulation,” no. July, 2017. [Online]. Available: <http://arxiv.org/abs/1707.07259>
- [24] M. Tucci, S. Rivero, and G. Ferrari-Trecate, “Line-Independent Plug-and-Play Controllers for Voltage Stabilization in DC microgrids,” *IEEE Transactions on Control Systems Technology*, pp. 1–9, 2016.

- [25] M. S. Sadabadi, Q. Shafiee, and A. Karimi, "Plug-and-Play Robust Voltage Control of DC Microgrids," *IEEE Transactions on Smart Grid*, pp. 1–1, 2017.
- [26] J.-J. Slotine and W. Li, *Applied Nonlinear Control*, 1991.
- [27] V. Nasirian, S. Moayedi, A. Davoudi, and F. Lewis, "Distributed Cooperative Control of DC Microgrids," *IEEE Transactions on Power Electronics*, vol. 8993, no. c, pp. 1–1, 2014.
- [28] S. Augustine, M. K. Mishra, and N. Lakshminarasamma, "Adaptive droop control strategy for load sharing and circulating current minimization in low-voltage standalone DC microgrid," *IEEE Transactions on Sustainable Energy*, vol. 6, no. 1, pp. 132–141, 2015.
- [29] X. Lu, K. Sun, J. M. Guerrero, J. C. Vasquez, and L. Huang, "State-of-Charge Balance Using Adaptive Droop Control for Distributed Energy Storage Systems in DC Microgrid Applications," *IEEE Trans. Ind. Electron.*, vol. 61, pp. 2804–2815, 2014.
- [30] T. Dragicevic, J. M. Guerrero, J. C. Vasquez, and D. Skrlec, "Supervisory control of an adaptive-droop regulated DC microgrid with battery management capability," *IEEE Transactions on Power Electronics*, vol. 29, no. 2, pp. 695–706, 2014.
- [31] V. Nasirian, A. Davoudi, F. L. Lewis, and J. M. Guerrero, "Distributed adaptive droop control for DC distribution systems," *IEEE Transactions on Energy Conversion*, vol. 29, no. 4, pp. 944–956, 2014.
- [32] B. D. Anderson, "Failures of adaptive control theory and their resolution," *Communications in Information and Systems*, vol. 5, no. 1, pp. 1–20, 2005.
- [33] T. E. Gibson, A. M. Annaswamy, and E. Lavretsky, "Improved Transient Response in Adaptive Control Using Projection Algorithms and Closed Loop Reference Models," *AIAA Guidance, Navigation, and Control Conference*, no. August, pp. 1–13, 2012.
- [34] C. Cao and Hovakimyan, *L1 Adaptive Control Theory: Guaranteed Robustness with Fast Adaptation*. Society for Industrial and Applied Mathematics, 2010.
- [35] T. V. Vu, D. Perkins, F. Diaz, D. Gonsoulin, C. S. Edrington, and T. El-Mezyani, "Robust adaptive droop control for DC microgrids," *Electric Power Systems Research*, vol. 146, pp. 95–106, 2017.
- [36] T. V. Vu, D. Perkins, B. Papari, C. S. Edrington, and A. L. Review, "Distributed Adaptive Control Design for Cluster of Converters in DC Distribution Systems," *2nd IEEE International Conference on DC Microgrids (ICDCM 2017)*, pp. 197–201, 2017.
- [37] B. Michini and J. P. How, "L1 adaptive control for indoor autonomous vehicles: Design process and flight testing," *Proceeding of AIAA Guidance, Navigation, and Control Conference*, no. August, pp. 1–15, 2009.
- [38] I. Gregory, E. Xargay, C. Cao, and N. Hovakimyan, "Flight Test of an L1 Adaptive Controller on the NASA AirSTAR Flight Test Vehicle," *AIAA Guidance, Navigation, and Control Conference*, pp. 1–31, 2010.
- [39] C. H. Svendsen, N. O. Holck, R. Galeazzi, and M. Blanke, "L1 adaptive manoeuvring control of unmanned high-speed water craft," *IFAC Proceedings Volumes (IFAC-PapersOnline)*, vol. 9, no. PART 1, pp. 144–151, 2012.
- [40] Z. Li, N. Hovakimyan, C. Cao, and G.-o. Kaasa, "Integrated Estimator and L1 Adaptive Controller for Well Drilling Systems," in *American Control Conference*, 2009, pp. 1958–1963.
- [41] H. Zhao, Q. Wu, C. N. Rasmussen, and M. Blanke, "L1 Adaptive Speed Control of a Small Wind Energy Conversion System for Maximum Power Point Tracking," *IEEE Transactions on Energy Conversion*, vol. 29, no. 3, pp. 576–584, 2014.

- [42] G. Kumaresan and A. Kale, “Application of L1 adaptive controller for the design of a novel decentralized leader follower formation algorithm,” *IFAC-PapersOnLine*, vol. 49, no. 1, pp. 706–711, 2016.
- [43] I. S. 1159-1995, *IEEE Recommended Practice for Monitoring Electric Power Quality*, 1995, vol. 2009, no. June.
- [44] D. O’Keeffe, S. Rivero, L. Albiol-Tendillo, and G. Lightbody, “Voltage Control of DC Islanded Microgrids : Scalable Decentralised L1 Adaptive Controllers,” 2018. [Online]. Available: [arXivpreprintarXiv:1801.04508](#)
- [45] N. B. Siraskar, “Decentralised Control of Large Scale Interconnected Systems with Application to Web Processing Machine,” Ph.D. dissertation, Oklahoma State University, 2004.
- [46] P. R. Pagilla, R. V. Dwivedula, and N. B. Siraskar, “A decentralized model reference adaptive controller for large-scale systems,” *IEEE/ASME Transactions on Mechatronics*, vol. 12, no. 2, pp. 154–163, 2007.
- [47] D. O’Keeffe, S. Rivero, L. Albiol-Tendillo, and G. Lightbody, “Global Asymptotic Stability for General MIMO Distributed Systems : An Approach Based on Robust-Adaptive Controllers,” 2018. [Online]. Available: [arXivpreprintarXiv:1801.02331](#)
- [48] F. Dorfler and F. Bullo, “Kron reduction of graphs with applications to electrical networks,” *IEEE Transactions on Circuits and Systems I: Regular Papers*, vol. 60, no. 1, pp. 150–163, 2013.
- [49] C. Aboky, G. Sallet, and J. C. Vivalda, “Observers for Lipschitz non-linear systems,” *International Journal of Control*, vol. 75, no. 3, pp. 204–212, 2002.
- [50] X. Lu, J. M. Guerrero, K. Sun, and J. C. Vasquez, “An improved droop control method for dc microgrids based on low bandwidth communication with dc bus voltage restoration and enhanced current sharing accuracy,” *IEEE Transactions on Power Electronics*, vol. 29, no. 4, pp. 1800–1812, 2014.